Received: 19 August 2018 | Accepted: 15 November 2018

DOI: 10.1111/jace.16231

Journal of the American Ceramic Society

ORIGINAL ARTICLE

Phase transition, microstructure and electrical properties of $K_{1-x}Na_xNbO_3$-based ceramic sintered in reducing atmosphere

Zhenyong Cen | **Yichao Zhen** | **Wei Feng** | **Lingling Chen** | **Peiyao Zhao** | **Yan Yu** | **Mengjian Xiao** | **Longtu Li** | **Xiaohui Wang**

State Key Laboratory of New Ceramics and Fine Processing, School of Materials Science and Engineering, Tsinghua University, Beijing, China

Correspondence
Xiaohui Wang, State Key Laboratory of New Ceramics and Fine Processing, School of Materials Science and Engineering, Tsinghua University, Beijing, China.
Email: wxh@tsinghua.edu.cn

Abstract

Lead-free $0.955K_{1-x}Na_xNbO_3$-$0.045Bi_{0.5}Na_{0.5}ZrO_3$+0.4% mol MnO ceramics (Abbreviated as $K_{1-x}N_xN$-0.045BNZ+0.4Mn) were prepared by a conventional solid-state sintering method in a reducing atmosphere (oxygen partial pressure p_{O_2}: 1×10^{-11} MPa). All $K_{1-x}N_xN$-0.045BNZ+0.4Mn samples show a pure perovskite structure with a polymorphic phase boundary (PPB) composed of rhombohedral (R) and tetragonal (T) phases. A high Na/K ratio and a low Na/K ratio can both induce an increase in the rhombohedral phase. The reverse piezoelectric coefficient d_{33}^* and its temperature stability in $K_{1-x}N_xN$-0.045BNZ+0.4Mn ceramics can be improved by controlling the Na/K ratio. The increase in the Na/K ratio from $x = 0.46$ to $x = 0.56$ can decrease the A-site cation vacancies. The activation energy of the grain is higher than that of the grain boundary due to the accumulation of oxygen vacancies at the grain boundary. $K_{1-x}N_xN$-0.045BNZ+0.4Mn ceramics with excellent piezoelectric properties (quasi-static piezoelectric coefficient $d_{33} = 326$ pC/N, and $d_{33}^* = 472$ pm/V at $E_{max} = 25$ kV/cm) were obtained at $x = 0.52$.

1 | INTRODUCTION

Piezoelectric ceramics are widely used in various devices, such as sensors, actuators, and transducers. $Pb(Zr_{1-x}Ti)O_3$(PZT)-based ceramics have dominated the whole piezoelectric market for many years. However, the application of lead-based ceramics has been restricted because of the high toxicity of lead oxide.[1] Thus, it is urgent to develop lead-free piezoelectric devices to replace lead-based devices. At present, KNN-based ceramics are studied by many investigators and have been considered a promising lead-free system to replace lead-based ceramics because of their environmental friendliness, excellent piezoelectric properties and high Curie temperature.[2–4]

Multilayer piezoelectric actuators have been widely used in precision equipment. In the current market, the internal electrode of the multilayer actuator is a silver palladium electrode.[5] As these actuators are an engineering solution, we must pay attention to the manufacturing cost. The market price of silver palladium electrodes as the inner electrode is very expensive, which is not conducive to the reduction in the material costs. The use of precious metal electrodes dramatically improves the cost of piezoelectric devices. Nickel electrodes have a significant cost advantage compared with precious metals.

In addition to the greater cost effectiveness, nickel electrodes have a high electromigration resistance and a high interfacial strength with ceramics. To reach cost reduction and environmental conservation goals, we consider that $K_{0.5}Na_{0.5}NbO_3$-based multilayer piezoelectric actuators with nickel electrodes should be adopted. However, ceramics with nickel electrodes must be sintered in a reducing atmosphere due to their weak oxidation resistance.[6,7] Thus, the design and preparation of KNN-based ceramics with

excellent reduction-resistant and piezoelectric properties is the most important task at present.

To date, few studies on $K_{0.5}N_{0.5}NbO_3$-based ceramics sintered in a reducing atmosphere have been reported. We successfully prepared $0.955K_{0.5}Na_{0.5}NbO_3$-$0.045Bi_{0.5}Na_{0.5}ZrO_3$+0.4% mol MnO (KNN-0.045BNZ+0.4Mn) ceramics sintered in a reducing atmosphere (oxygen partial pressure p_{O_2}: 1×10^{-11} MPa) with excellent piezoelectric properties ($d_{33}^* = 430$ pm/V at $E = 25$ kV/cm and $d_{33} = 300$ pC/N).[8] Meanwhile, the temperature stability (~60°C) of the reverse piezoelectric coefficient (d_{33}^*) of KNN-0.045BNZ+0.4Mn ceramics is not suitable for application. After that, $0.955K_{0.5}Na_{0.5}Nb_{0.98}Ta_{0.02}O_3$-$0.045Bi_{0.5}Na_{0.5}ZrO_3$+0.4% mol MnO show a higher temperature stability (~80°C) of d_{33}^* and a better d_{33}^* (475 pm/V at $E = 25$ kV/cm) due to the complexity of smaller nanodomains (~70 nm) that formed inside larger submicron domains (~200 nm).[9] After considering the cost of materials, we hope to achieve good properties in a simple manner due to the price of Ta_2O_5. There is a close relationship between the temperature stability of piezoelectric properties and the polycrystalline phase transition (PPT). In the literatures, the piezoelectric properties and PPT of KNN-based ceramics are very strongly dependent on their K/Na ratios.[10–13] Thus, we expect that the piezoelectric properties and the temperature stability of KNN-0.045BNZ +0.4Mn ceramics can be improved by controlling the K/Na ratio. In this research, the evolutionary mechanism of the phase structure, piezoelectric properties and temperature stability of d_{33}^* for $0.955K_{1-x}Na_xNbO_3$-$0.045Bi_{0.5}Na_{0.5}ZrO_3$+0.4% mol MnO ceramics sintered in a reducing atmosphere were investigated.

2 | EXPERIMENTAL PROCEDURES

$0.955K_{1-x}Na_xNbO_3$-$0.045Bi_{0.5}Na_{0.5}ZrO_3$+0.4% mol MnO ($K_{1-x}N_xN$-0.045BNZ+0.4Mn) ($x$=0.46, 0.48, 0.50, 0.52, 0.54 and 0.56) piezoelectric ceramics sintered in a reducing atmosphere ($H_2/N_2/H_2O$, oxygen partial pressure: $p_{O_2} = 1 \times 10^{-11}$ MPa) were prepared by conventional solid-state reaction methods, as described elsewhere.[8]

Crystal structures of $K_{1-x}N_xN$-0.045BNZ+0.4Mn ceramic were detected using x-ray diffraction (XRD) equipment (Rigaku 2500, Rigaku, Tokyo, Japan). The samples were polished and were treated by hot corrosion at 1060°C for 30 minutes. A scanning electron microscopy (SEM) (MERLIN VP Compact, Zeiss Ltd, Germany) was used to observe the surface microstructures of the ceramics. The domain morphology of ceramics was observed on transmission electron microscope (Tecnai G2 F20 S-TWIN, FEI, America).

The ion sputtering equipment (SBC-12, KYKY Technology Co, Beijing, China) was used to sputter gold electrodes on the samples. The samples were poled under a dc field of 35 kV/cm for 20 minutes in a silicone oil bath at room temperature. The poled samples were placed for 3 days and its d_{33} was measured using a Berlincourt d_{33} meter (ZJ-6A, Institute of Acoustics, Chinese Academy of Sciences, Beijing, China). Piezoelectric and dielectric properties at room temperature were tested using an impedance analyzer (Agilent 4294A, Agilent, Santa Clara, CA). The temperature dependence of electric-field-induced strain (S-E) curves was measured in situ using the ferroelectric analyzer (aixACCT Systems GmbH, Aachen, Germany) in the temperature range from 25 to 110°C. Impedance measurements above 300°C at a frequency range from 20 Hz to 2 MHz with an AC measurement voltage of 0.1 V were measured using a capacitance meter (HP4980A, Hewlett-Packard) with an automated temperature controller (HDMS-1000, Partulab Technology, Wuhan, China).

3 | RESULTS AND DISCUSSION

Figure 1A shows XRD patterns of $K_{1-x}N_xN$-0.045BNZ+0.4Mn ceramics at a 2θ range of 10°-120°. We find that all ceramics show a pure perovskite structure, which suggests that a stable solid solution is formed when $x = 0.46$-0.56. In Figure 1B, the XRD patterns of the ceramics show that the change in the Na/K ratio can induce a structural form transition. Figure 1C shows that the diffraction peak moves to a high angle when x increases from 0.46 to 0.56. This suggests that the cell volume of samples contracts with increasing x values from 0.46 to 0.56 because the ionic radius (1.64 Å:12 CN) of K^+ ions is larger than that (1.39 Å:12 CN) of Na^+ ions.[14]

Rietveld refinement is carried out for the XRD data of powder from all the ceramics to obtain their structural parameters. The lattice parameters, phase fraction (PF) and space group (SG) of $K_{1-x}N_xN$-0.045BNZ+0.4Mn ceramics are listed in Table 1. A PPB with R and T phases exists in all samples. The SG of the T and R phases are P4 mm and R3 m, respectively. In Table 1, we find that when x decreases from 0.50 to 0.46, the PF of the R phase increases from 18.11% to 27.56%. Meanwhile, the PF of the R phase also increases from 18.11% to 38.56% with increasing x values from 0.50 to 0.56. This suggests that the PF of the R and T phases for KNN-0.045BNZ+0.4Mn ceramics can be controlled by changing the K/Na ratio.

Figure 2 shows TEM micrographs of $K_{1-x}N_xN$-0.045BNZ+0.4Mn ceramics. Large domains and small domains are adjacent to each other. We found that the submicron-size lamellar domains (~100 nm) of ceramics exist at $x = 0.50$. We found that the submicron-size domains (~100 nm) and nanoscale domains (~60 nm) coexist in ceramics at $x = 0.48$. When x decreases from 0.48 to 0.46, the submicron domain size increases from ~100 to 180 nm,

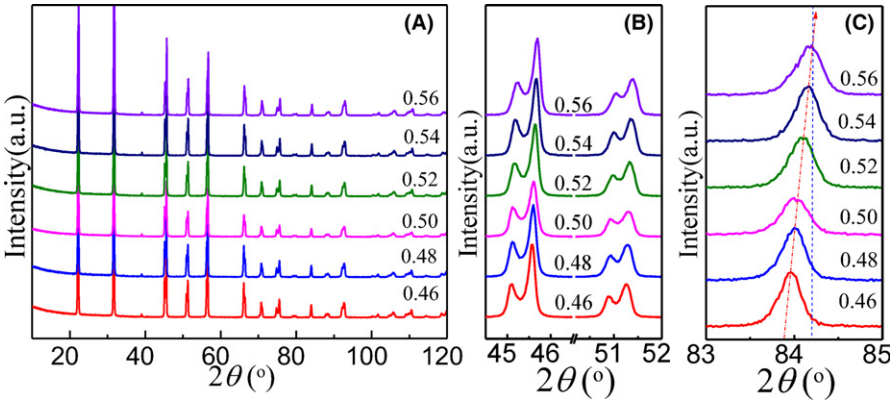

FIGURE 1 Room-temperature XRD patterns of $K_{1-x}N_xN$-0.045BNZ+0.4Mn ceramics (A) at 2θ=10°-120° (B) at 2θ=44°-52° (C) at 2θ=83°-85° [Color figure can be viewed at wileyonlinelibrary.com]

and the nanodomain size increases from ~60 to ~90 nm. Meanwhile, when x increases from 0.52 to 0.56, the submicron domain size increases from ~130 to 160 nm, and the nanodomain size increases from ~30 to ~90 nm. In contrast to the complex domain structure of the $0.955K_{0.5}Na_{0.5}Nb_{0.98}Ta_{0.02}O_3$-$0.045Bi_{0.5}Na_{0.5}ZrO_3$+0.4% mol MnO system, the large submicron domains and small nanodomains are arranged side by side in $K_{1-x}N_xN$-0.045BNZ+0.4Mn ceramics. In the polymorphic phase boundary (PPB), the disappearance of polar anisotropy is beneficial to the generation of nanodomains due to the optimal ratio of the T phase and R phase,[15] which enhances the piezoelectric properties. We consider that the reason for this phenomenon is rather complicated and is most likely due to the increase in the R phase, which needs further study.

Figure 3A shows the ferroelectric hysteresis loop of $K_{1-x}N_xN$-0.045BNZ+0.4Mn ceramics. The saturated electric hysteresis loops of all ceramics show that they are typical ferroelectrics at $x = 0.46$-0.56. In Figure 3 (b), the remanent polarization (Pr) changes with the change in the ratio of Na/K. The Pr of samples at $x = 0.48$ and 0.52 shows an increase due to the formation of smaller nanodomains. The Pr at $x = 0.52$ shows its maximal value, which is attributed to the existence of smaller domains (~30 nm). The smallest nanodomains (~30 nm) form in similar grains due to the optimal R phase content (~22.33%), which induces easy switching by an electric field.

The quasi-static piezoelectric coefficient (d_{33}), density (ρ), plane electromechanical coupling coefficient (k_p) and phase transition temperature ($T_{R\text{-}T}$) for $K_{1-x}N_xN$-0.045BNZ+0.4Mn ceramics are listed in Table 2. Optimal d_{33} (326 pC/N) is obtained at $x = 0.52$. The piezoelectric constant d_{33} is calculated by Equation (1).[16]

$$d_{33} = 2Q\varepsilon_0\varepsilon_{33}P_3 \quad (1)$$

Q refers to the electrostrictive constant and varies little with changing temperature.[17] ε_0 refers to the vacuum dielectric constant. ε_{33} refers to the dielectric constant. P_3 refers to the polarization along the polar axis and approximates the remanent polarization P_r of ferroelectric ceramics. In Figure 3, the highest P_r of samples is obtained at $x = 0.52$, which is responsible for optimal d_{33} (326 pC/N). The density (ρ) decreases with increasing x from 0.46 to 0.56. The contribution of nanodomains is the origin of the high piezoelectric property of KNN-based ceramic, which has been verified.[18] Thus, relatively high d_{33} values of 310 pC/N and 326 pC/N are obtained at $x = 0.48$ and $x = 0.52$, respectively, due to the formation of ~60 and ~30 nm nanodomains.

The temperature dependence of the dielectric constant ε_r and dielectric loss tan δ at 1 kHz for $K_{1-x}N_xN$-0.045BNZ+0.4Mn ceramics in the temperature range of 25-450°C is shown in Figure S1A. There is no change in Curie temperature (T_C) observed at $x = 0.46$-0.56. The T_C of all the samples is ~340°C. The temperature dependence of the dielectric constant ε_r at 1 kHz for $K_{1-x}N_xN$-0.045BNZ+0.4Mn ceramics in the temperature range of 25-180°C is shown in Figure S1B. The phase transition temperature ($T_{R\text{-}T}$) between the R phase and T phase was changed by controlling the Na/K ratio. The $T_{R\text{-}T}$ of all samples is listed in Table 2. At $x = 0.46$-0.56, the $T_{R\text{-}T}$ decreases from 87 to 72°C and then increases from 77 to 92°C. The increase in $T_{R\text{-}T}$ is due to the increase in the R phase.

Figure 4 shows the unipolar S-E curves and reverse piezoelectric coefficient d^*_{33} for the $K_{1-x}N_xN$-0.045BNZ+0.4Mn ceramics measured at a frequency of 1 Hz. In Figure 5, the unipolar strain-electric field can be improved by controlling the Na/K ratio. The reverse piezoelectric coefficient was calculated via the Equation $d^*_{33} = S_{max}/E_{max}$. In the inset of Figure 4, the reverse piezoelectric coefficient d^*_{33} as a function of E_{max} for all ceramics is shown. Large d^*_{33} values of 452 pm/V and 472 pm/V (at $E_{max} = 25$ kV/cm) are obtained for ceramics at $x = 0.48$ and $x = 0.52$, respectively, which should result from the contribution of smaller nanodomains, as shown in Figure 2. Further increases of the R phase cause the d^*_{33} of the samples at $x > 0.52$ and $x < 0.48$ to decrease. Reverse piezoelectric coefficient d^*_{33}, insulation resistivity, Curie temperatures T_C and oxygen partial pressure p_{O_2} of the KNN-based ceramic sintered in a reducing atmosphere are

TABLE 1 Lattice parameters, phase fraction (PF) and space group (SG) of $K_{1-x}N_xN$-0.045BNZ+0.4Mn ceramics

	$x = 0.46$		$x = 0.48$		$x = 0.50$		$x = 0.52$		$x = 0.54$		$x = 0.56$	
a (Å)	3.978	3.999	3.978	3.997	3.976	4.003	3.971	3.988	3.970	3.984	3.970	3.982
b (Å)	3.978	3.999	3.978	3.997	3.976	4.003	3.971	3.988	3.970	3.984	3.970	3.982
c (Å)	4.017	3.999	4.016	3.997	4.013	4.003	4.010	3.988	4.010	3.984	4.008	3.982
SG	P4mm	R3m	P4mm	R3m	P4mm	R3m	P4mm	R3m	P4mm	R3m	P4mm	R3m
PF (%)	~71.44	~28.56	~75.13	~24.87	~81.89	~18.11	~77.67	~22.33	~73.27	~26.73	~61.44	~38.56

listed in Table 3. In Table 3, we find that the ceramics at $x = 0.52$ show the largest d_{33}^* value (472 pm/V) among $K_{0.5}Na_{0.5}NbO_3$-based systems sintered in a reducing atmosphere.

The temperature dependence of the reverse piezoelectric coefficient (d_{33}^*) of the poled (35 kV/cm)/aged (3 days) $K_{1-x}N_xN$-0.045BNZ+0.4Mn ceramics was measured in situ at a frequency of 1 Hz and 35 kV/cm as shown in Figure 5. The temperature sensitivity of d_{33}^* can be evaluated by the value η, as shown in the following Equation [η (%) = (d_{33}^* (*T*)- d_{33}^* (25°C) × 100)/d_{33}^* (25°C)]. In practical applications, η should be controlled to within −10% to +10% or less.[28] When η exceeds the limit range the temperature is marked as T_e. As shown in Figure 6, when *x* increases from 0.50 to 0.56, T_e increases from 60 to 100°C. However, T_e shows a decrease at $x = 0.46$. The larger domains at $x < 0.50$ and $x > 0.50$ appear due to the increase in the R phase. We consider that larger domains need a greater activation energy, which can result in poor temperature sensitivity of d_{33}^* at high temperatures. Thus, the T_e increases at $x = 0.50$-0.56. However, the appearance of large domains in ceramics at $x = 0.46$ does not enhance the temperature stability of d_{33}^*. We consider that the increase in oxygen vacancy concentration may be responsible for the deterioration of temperature stability. The stability of ferroelectrics can be enhanced due to the decrease in oxygen vacancy concentration.[22] For $0.955K_{0.5}Na_{0.5}NbO_3$-$0.045Bi_{0.5}Na_{0.5}ZrO_3$+*y* %MnO systems, 0.4% mol MnO ions occupy the A-site cation vacancies.[8,23,24] We consider that some Mn^{2+} ions in the A-site have switched to the B-site at $x = 0.46$, as shown in Equation (2).

$$MnO \overset{ZrO_2}{\leftrightarrow} Mn''_{Zr} + V_O^{\bullet\bullet} + O_O \quad (2)$$

From the stability of the perovskite structure, we consider that a smaller difference between the ionic radius of the doped ions and ionic radius of the matrix ions corresponds to higher stability of the perovskite structure due to smaller lattice distortion. The difference in radii (0.11 Å) between Mn^{2+} ions (0.83 Å: 6CN) and Zr^{4+} ions (0.72 Å: 6CN) is less than the difference in radii (0.19 Å) between Mn^{2+} ions (0.83 Å: 6CN) and Nb^{5+} ions (0.64 Å: 6CN).[14,25] Thus, Mn^{2+} ions should substitute for Zr^{4+} ions from $x = 0.48$ to $x = 0.46$. As shown in formula (2), new oxygen vacancies ($V_{\ddot{O}}$) form, which increases the oxygen vacancies. Thus, the stability of ferroelectrics for samples at $x = 0.46$ deteriorates, which results in a decrease in *T*e.

The impedance spectra of $K_{1-x}N_xN$-0.045BNZ+0.4Mn ceramics measured at different temperatures are shown in Figure 6. *Z*′ and *Z*″ refer to the real and imaginary parts of the complex impedance Z*. We find that the Na/K ratio has a significant effect on impedance spectra of $K_{1-x}N_xN$-0.045BNZ+0.4Mn ceramics. The fitted resistance (R) of each component is used to calculate the activation energy of conduction (*E*a) using Arrhenius' law. A tail of impedance spectra at low frequencies is enhanced gradually when the measured temperature increases. The formation of a "tail" may result from the contribution of the ionic conduction of alkaline ion vacancies.[26] Meanwhile, we can observe that the "tail" can disappear at a high Na/K ratio, which is similar to findings in the literature.[27] This suggests that an increase in the Na/K ratio can induce a decrease in alkaline ion vacancies. Thus, we believe that the oxygen vacancy concentration that is due to the loss of alkaline ions would decrease with increasing *x*.

The equivalent electrical circuit of $K_{1-x}N_xN$-0.045BNZ+0.4Mn ceramics is shown in Figure 7A. Meanwhile an equivalent electrical circuit comprising two RC circuits (R parallel to C) connected in series (shown in Figure 7A) was used to model the impedance experimental data in Zview software. The resistance of the grain (R_g) and the grain boundary (R_{gb}) in $K_{1-x}N_xN$-0.045BNZ+0.4Mn ceramics are listed in Table S1. The capacitance of grain (C_g) and grain boundary (C_{gb}) for $K_{1-x}N_xN$-0.045BNZ+0.4Mn ceramics are listed in Table S2. The activation energy of the grain and the grain boundary for $K_{1-x}N_xN$-0.045BNZ+0.4Mn ceramics are shown in Figure 7B. We find that the resistance of the grain boundary (R_{gb}) is lower than the resistance of the grain (R_g), as shown in Table S1. In Table S2, we find that the C_{gb} for all samples is higher than the Cg. In Figure 7B, we find that the activation energy (E_{gb}) of the grain boundary for all samples is lower than the activation energy (E_g) of the grain. The similar and anomalous phenomena observed for some Ti-rich $Sr_{0.995}Ti_1O_3$ ceramics sintered in air with smaller

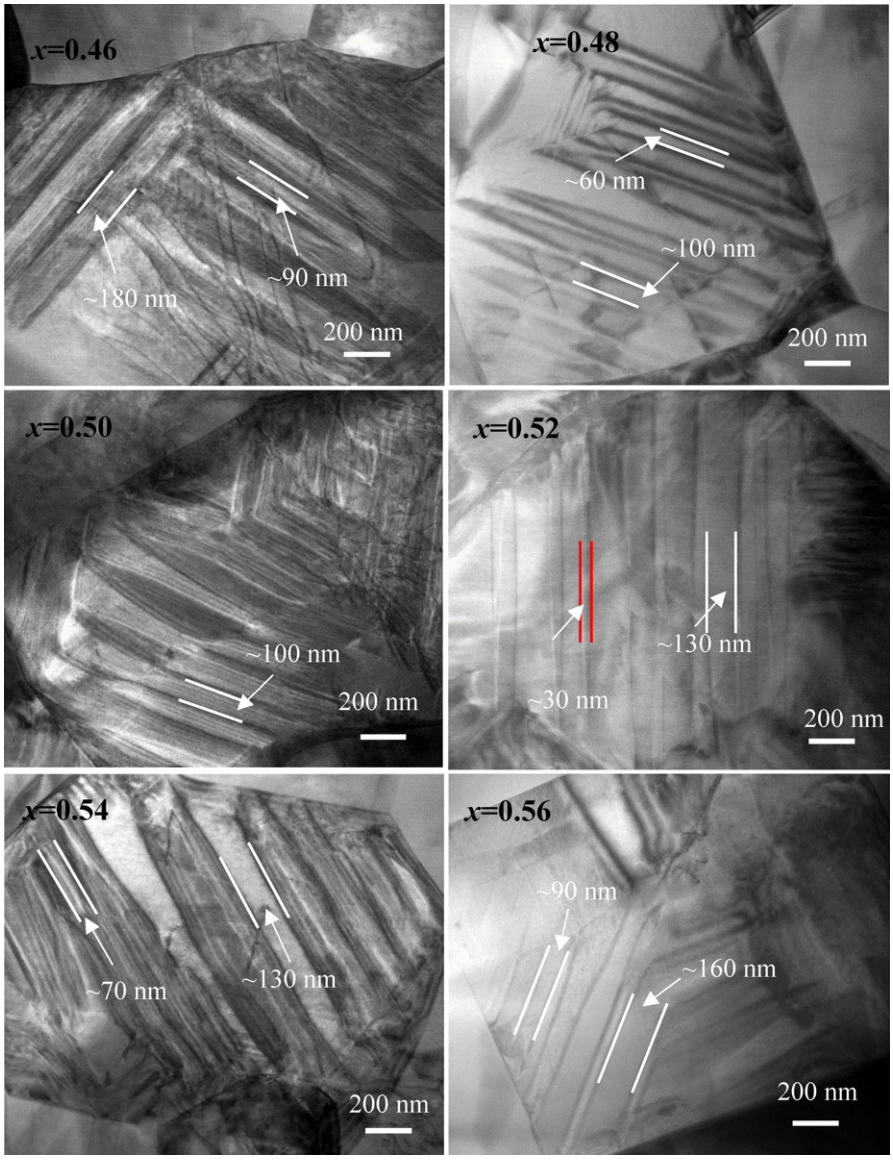

FIGURE 2 TEM micrographs of $K_{1-x}N_xN$-0.045BNZ+0.4Mn ceramics [Color figure can be viewed at wileyonline library.com]

grain size are due to the large specific area of grain boundary and high oxygen vacancy concentration.[28,29] The KNN-based ceramics are extremely prone to similar phenomena that Nb-rich KNN-based ceramics are due to the high volatilization in the A-site. Meanwhile, the sintering difficulty of KNN-based ceramics results from the difficulty in ion diffusion not being

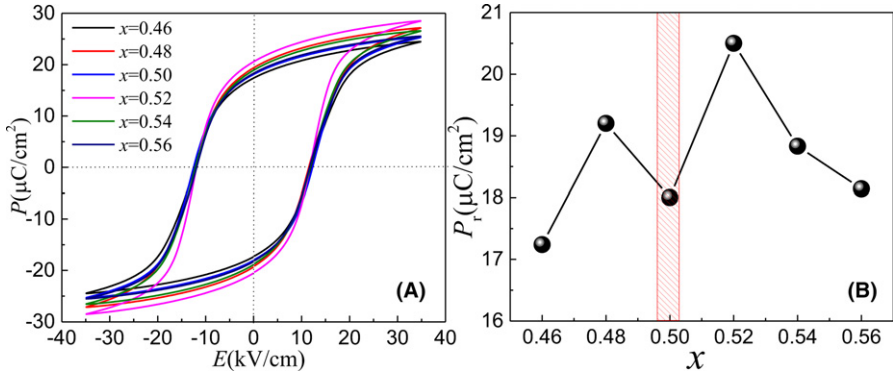

FIGURE 3 A, Ferroelectric hysteresis loop of $K_{1-x}N_xN$-0.045BNZ+0.4Mn ceramics (B) Remanent polarization of $K_{1-x}N_xN$-0.045BNZ+0.4Mn ceramics [Color figure can be viewed at wileyonlinelibrary.com]

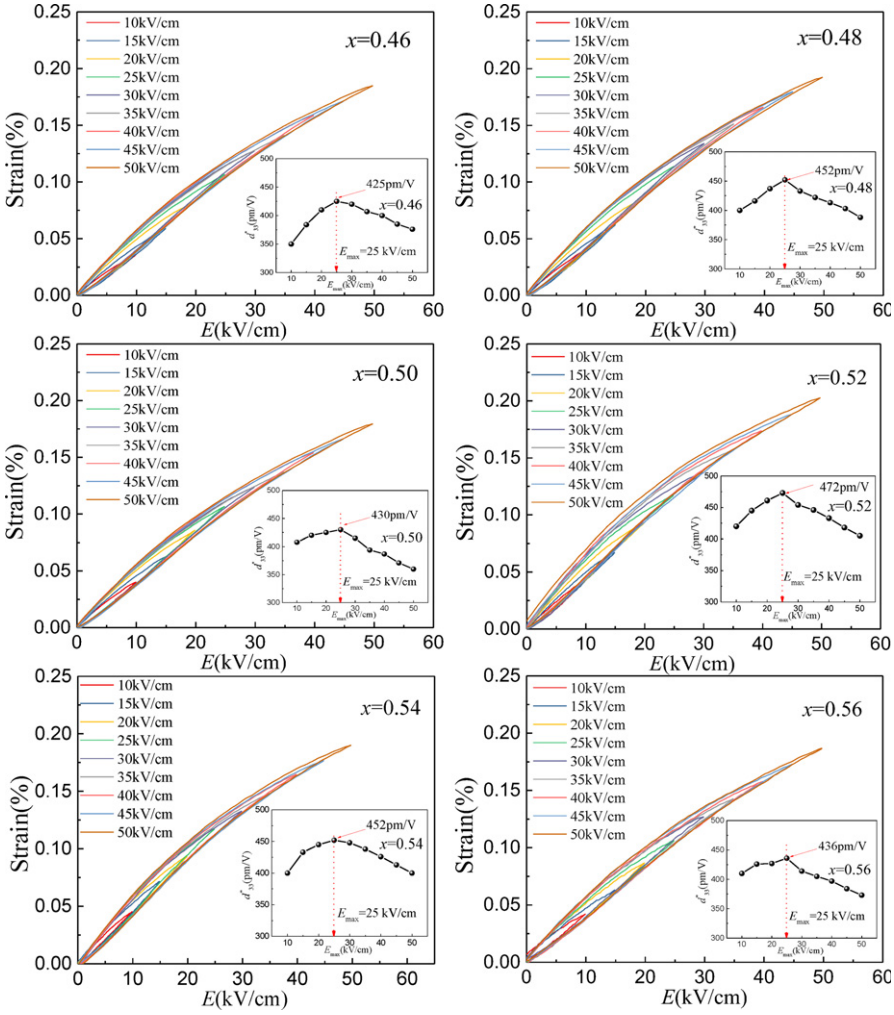

FIGURE 4 Unipolar strain-electric field (S-E) curves and reverse piezoelectric coefficient d^*_{33} for the poled (35 kV/cm)/aged (3 d) $K_{1-x}N_xN$-0.045BNZ+0.4Mn ceramics measured at a frequency of 1 Hz [Color figure can be viewed at wileyonlinelibrary.com]

TABLE 2 Quasi-static piezoelectric constant (d_{33}), density (ρ), plane electromechanical coupling coefficient (k_p) and phase transition temperature ($T_{R\text{-}T}$) for $K_{1-x}N_xN$-0.045BNZ+0.4Mn ceramics

	$x = 0.46$	$x = 0.48$	$x = 0.50$	$x = 0.52$	$x = 0.54$	$x = 0.56$
d_{33} (pC/N)	280	310	300	326	300	290
ρ (g/cm^3)	4.486	4.466	4.413	4.353	4.348	4.334
k_p (%)	47.1	48.7	51.2	56.2	54.3	52.1
$T_{R\text{-}T}$	87	82	72	77	81	92

conducive to grain growth. Thus, we consider that $K_{1-x}N_xN$-0.045BNZ+0.4Mn ceramics should possess the condition of $E_{gb} < E_g$.

Through further analysis, we consider that the $K_{1-x}N_xN$-0.045BNZ+0.4Mn ceramics sintered in a reducing atmosphere form many oxygen vacancies, as shown in Equation (3).

$$O_O^* \rightarrow \frac{1}{2}O_2 \uparrow + V_O^{\bullet\bullet} + 2e' \quad (3)$$

The escape of oxygen ions begins at the grain boundary. Thus, the concentration of oxygen vacancies in the grain boundary is higher than those in grain. During the cooling process, oxygen vacancies caused by volatilization subsequently do not oxidize under a reducing atmosphere,

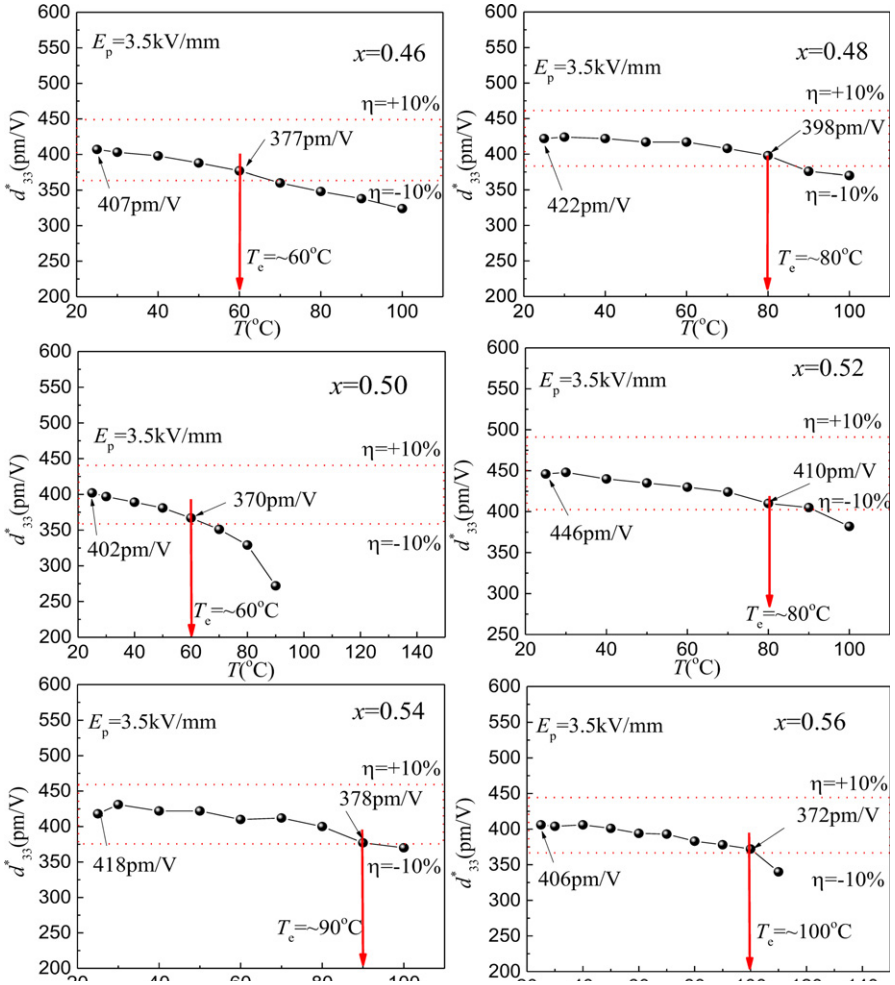

FIGURE 5 Temperature dependence of reverse piezoelectric coefficient (d^*_{33}) for the poled (35 kV/cm)/aged (3 d) $K_{1-x}N_xN$-0.045BNZ+0.4Mn ceramics in situ measured at a frequency of 1 Hz and 35 kV/cm [Color figure can be viewed at wileyonlinelibrary.com]

TABLE 3 Reverse piezoelectric coefficient d^*_{33}, insulation resistivity, Curie temperatures T_C and oxygen partial pressure p_{O_2} for KNN-based ceramic sintered in a reducing atmosphere

Composition	d^*_{33} (pm/V)	Resistivity (Ω·cm)	T_C (°C)	Oxygen partial pressure (p_{O_2})	Cite
$0.96(Na_{0.5}K_{0.5})NbO_3-0.04CaZrO_3$+0.03$ZrO_2$	360 (20 kV/cm)	6.3×10^{10}	~260	1×10^{-10}-1×10^{-11} MPa	[19]
x(NaF-0.5Nb_2O_5)-(1-x)[$Na_{0.5}K_{0.5}(Nb_{0.8}Ta_{0.2})O_3$]	~385 (50 kV/cm)	1.6×10^{10}	~296	1×10^{-7} atm	[20]
$(Na_{0.5}K_{0.5})NbO_3$–LiF	~200 (26 kV/cm)	2.7×10^{11}	~456	1×10^{-10} atm	[21]
$0.955K_{0.5}Na_{0.5}NbO_3-0.045Bi_{0.5}Na_{0.5}ZrO_3$+$x$%MnO	430 (25 kV/cm)	6.13×10^{11}	~335	1×10^{-10} atm	[8]
$0.955K_{0.5}Na_{0.5}Nb_{1-x}Ta_xO_3-0.045Bi_{0.5}Na_{0.5}ZrO_3$+0.4%MnO ($x$ = 0.02)	475 (25 kV/cm)	9.46×10^{11}	~336	1×10^{-10} atm	[9]
$0.955K_{1-x}Na_xNbO_3$-0.045$Bi_{0.5}Na_{0.5}ZrO_3$+0.4%MnO (x = 0.52)	473 (25 kV/cm)	9.62×10^{11}	~330	1×10^{-10} atm	This work

as shown in Equation (4), and the grain boundary is negatively charged.

$$\frac{1}{2}O_2 + V_O^{\bullet\bullet} \rightarrow O_O^* + 2h^{\bullet} \quad (4)$$

At higher temperatures ($T > 250$°C), the conduction of KNN-based ceramics is dominated by the motion of oxygen vacancies.[25] Thus, we consider that the contribution of oxygen vacancies to the decrease in resistance at the grain boundary is stronger than that in grain at $T > 300$°C. Thus, E_{gb} are both lower than E_g. The E_g first decreases and then increases with increasing x from 0.46 to 0.56. The ceramics at $x = 0.50$ show a minimum E_g value (0.73 eV). For all samples, when x increases

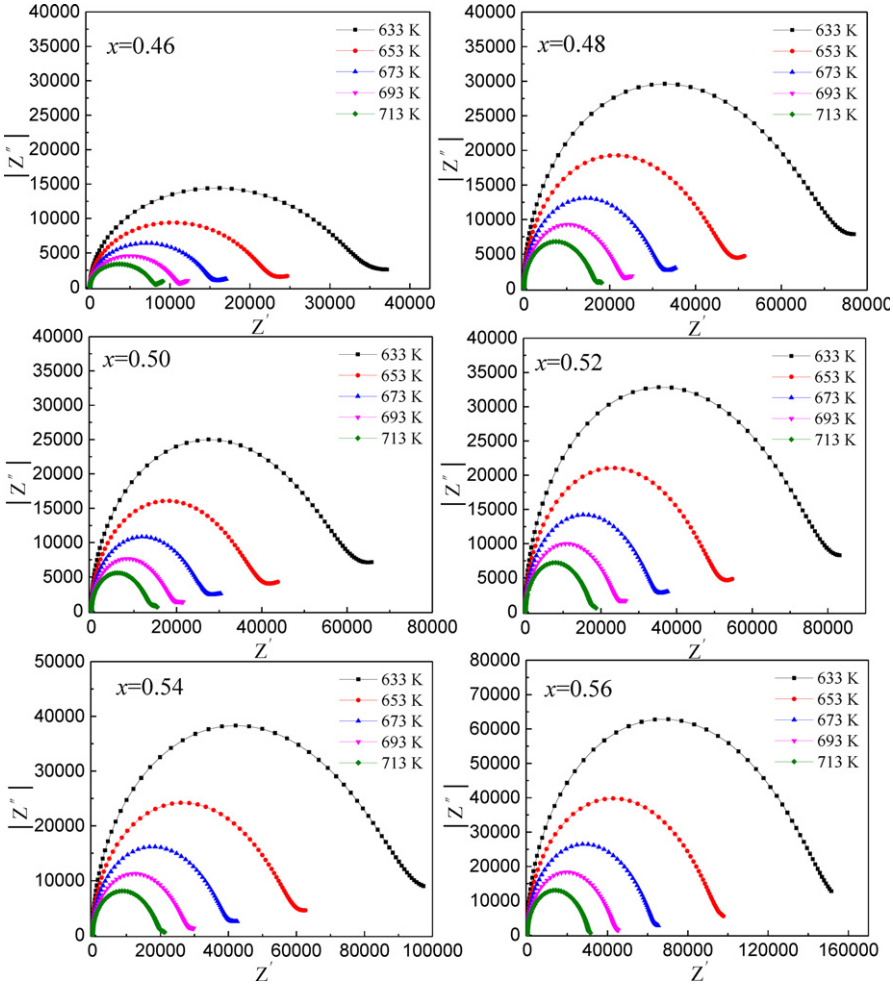

FIGURE 6 Impedance spectra of $K_{1-x}N_xN$-0.045BNZ+0.4Mn ceramics measured at different temperatures [Color figure can be viewed at wileyonlinelibrary.com]

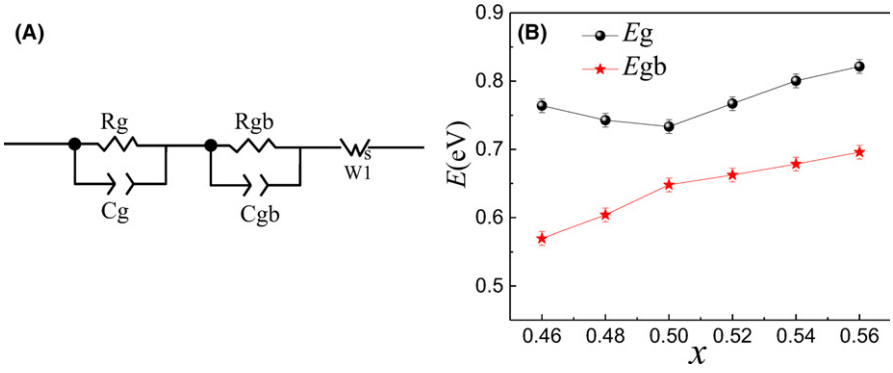

FIGURE 7 A, An equivalent electrical circuit of $K_{1-x}N_xN$-0.045BNZ+0.4Mn ceramics (B) Activation energy of grain and grain boundary for $K_{1-x}N_xN$-0.045BNZ+0.4Mn ceramics [Color figure can be viewed at wileyonlinelibrary.com]

from 0.46 to 0.56, E_{gb} obviously increases at $x = 0.46$-0.50 and E_{gb} slowly increases at $x = 0.52$-0.56. When x increases from 0.46 to 0.50, the ceramics show a decrease in E_g and an obvious increase in E_{gb}. We consider that when x decreases from 0.50 to 0.46, some Mn^{2+} ions in the A-site gradually change to the B-site, as shown in Equation (2). The additional oxygen vacancies form due to the substitution of Nb^{5+} ions with Mn^{2+} ions with decreasing x from 0.50 to 0.46, which induces an increase in E_g and an obvious decrease in E_{gb}.

On the one hand, the potential barrier height $\Delta\varphi_{gb}$ can be calculated by Equation (5) from the Schottky barrier model.[30] In Equation (5), [A′]refers to the acceptor concentration, Q_{gb} refers to the interface charge density per unit area and ε_0 and ε_{gb} refer to the dielectric constant of the vacuum and grain boundary, respectively.

$$\Delta\varphi_{gb} = \frac{Q_{gb}^2}{8\varepsilon_0\varepsilon_{gb}e[A']} \tag{5}$$

In the MnO-doped $0.955K_{0.5}Na_{0.5}NbO_3$-$0.045Bi_{0.5}Na_{0.5}ZrO_3$ system, 0.4% mol MnO ions preferentially

occupy the cation vacancies in the A-site.[8,23,24] The obvious decrease in E_{gb} for ceramics from $x = 0.50$ to $x = 0.46$ is likely caused by the occurrence of acceptor doping behavior, as shown in (2), because the increase in [A′] results in the decrease in barrier height $\Delta\varphi_{gb}$ (same as E_{gb}). On the other hand, Rgb is proportional to the thickness as follows (d_{gb}).[29]

$$R_{gb} = \left(\rho_{gb}\, d_{gb}\right)/A_{gb} \quad (6)$$

where ρ_{gb} refers to the resistivity of the grain boundary, A_{gb} refers to the area of the grain boundary and d_{gb} refers to the thickness of the grain boundary. Due to the decrease in oxygen vacancy, the d_{gb} of Ti-rich $Sr_{0.995}Ti_1O_3$ ceramics becomes thicker after annealing at 500°C in oxygen, resulting in an increase in the resistance of the grain boundary.[29] This suggests that the oxygen vacancies accumulated in the grain boundary can reduce the resistance owing to the decrease in d_{gb}. From $x = 0.50$ to $x = 0.46$, more additional oxygen vacancies with a positive charge move to the grain boundary with a negative charge, which decreases the thickness of the grain boundary and reduces the resistance of the grain boundary at high temperatures (633 K-713 K).[29] The increase in E_g from $x = 0.50$ to $x = 0.46$ can be attributed to the existence of a high dipole defect ($Mn''_{Zr} - V^{\bullet\bullet}_O$) concentration. The grain boundary with a negative effective charge repels the defects (Mn''_{Zr}) of a negative effective charge, which results in an increase in Mn''_{Zr}concentration in the interior of the grain. The defects with negative effective charge (Mn''_{Zr}) exist in grain interiors form the dipole defect ($Mn''_{Zr} - V^{\bullet\bullet}_O$). The $V^{\bullet\bullet}$ are bound by Mn''_{Zr} ions, which results in an increase in E_g from $x = 0.50$ to $x = 0.46$. Thus, we consider that a portion of Mn^{2+} ions in the A-site move to the B-site to substitute for Zi^{4+} ions from $x = 0.50$ to $x = 0.46$.

4 | CONCLUSIONS

Lead-free $0.955K_{1-x}Na_xNbO_3$-$0.045Bi_{0.5}Na_{0.5}ZrO_3$+0.4% MnO ceramics have been prepared by a conventional solid-state sintering method in a reducing atmosphere (oxygen partial pressure p_{O_2}: 1×10^{-11} MPa). At $x = 0.46$-0.56, the ceramics possess a PPB with R/T phase. A high Na/K ratio at $x > 0.5$ and a low Na/K ratio can both enhance the R phase. The piezoelectric properties and temperature stability of d^*_{33} of $K_{1-x}N_xN$-0.045BNZ+0.4Mn ceramics can be improved by controlling the Na/K ratio. Some original Mn^{2+} ions in the A-site move to the B-site to substitute for Zr^{4+} ions at $x = 0.46$, which results in a decrease in temperature stability due to the deterioration of ferroelectric stability. The increase in the Na/K ratio can decrease the A-site cation vacancies. For the $K_{1-x}N_xN$-0.045BNZ+0.4 Mn ceramics sintered in a reducing atmosphere, the E_{gb} is lower than the E_g because many oxygen vacancies accumulate in the grain boundary. The decrease in resistance in the grain boundary caused by oxygen vacancies is greater than that of the grain interior. Some Mn^{2+} ions from the A-site substitute for Zr^{4+} ions from $x = 0.50$ to $x = 0.46$, which results in an obvious decrease in E_{gb} and an increase in E_g. The optimal piezoelectric properties ($d_{33} = 326$ pC/N, and $d^*_{33} = 472$ pm/V at $E_{max} = 25$ kV/cm) of $K_{1-x}N_xN$-0.045BNZ+0.4Mn ceramics at $x = 0.52$ were obtained because the optimal ratio of the T phase and R phase is beneficial to weaken the polar anisotropy and generate smaller nanodomains (~30 nm).

ACKNOWLEDGMENT

The work was supported by National Natural Science Foundation of China (Grant No. 51672148), Ministry of Sciences and Technology of China through National Basic Research Program of China (973 Program 2015CB654604).

ORCID

Zhenyong Cen https://orcid.org/0000-0001-6143-9736
Wei Feng https://orcid.org/0000-0001-6856-9787
Lingling Chen https://orcid.org/0000-0001-9069-1471

REFERENCES

1. Zhang MH, Wang K, Du YJ, Dai G, Sun W, Li G, et al. High and temperature-insensitive piezoelectric strain in alkali niobate lead-free perovskite. J Am Chem Soc. 2017;139 (10):3889–95.
2. Wang Y, Liu Q, Wu J, Xiao D, Zhu J. Piezoelectric properties of (1-x)($Na_{0.5}K_{0.5}$)NbO_3-$x$$AgSbO_3$ lead-free ceramics. J Am Ceram Soc. 2009;92(3):755–7.
3. Zhang S-T, Kounga A B, Aulbach E, Ehrenberg H, Rödel J. Giant strain in lead-free piezoceramics $Bi_{0.5}Na_{0.5}TiO_3$-$BaTiO_3$-$K_{0.5}Na_{0.5}NbO_3$ system. Appl Phys Lett 2007;91(11):112906.
4. Xu K, Li J, Lv X, Wu J, Zhang X, Xiao D, et al. Superior piezoelectric properties in potassium-sodium niobate lead-free ceramics. Adv Mater. 2016;28(38):8519–23.
5. Huan Y, Wang X, Wei T, Xie JYZ, Zhao P, Li L. Defect engineering of high-performance potassium sodium niobate piezoelectric ceramics sintered in reduction atmosphere. J Am Ceram Soc. 2017;100(5):2024–33.
6. Sakabe Y, Minai K, Wakino K. High-dielectric constant ceramics for base metal monolithic capacitors. Jpn J Appl Phys. 1981;20 (S4):147–50.
7. Burn I, Maher GH. High resistivity $BaTiO_3$ ceramics sintered in CO-CO_2 atmospheres. J Mater Sci. 1975;10(4):633–40.
8. Cen Z, Wang X, Huan Y, Li L. Temperature stability and electrical properties of MnO-doped KNN-based ceramics sintered in reducing atmosphere. J Am Ceram Soc. 2018;101(6):2391–407.
9. Cen Z, Zhen Y, Feng W, Zhao P, Chen L, Zhu C, et al. Improving piezoelectric properties and temperature stability for KNN-based ceramics sintered in a reducing atmosphere. J Am Ceram Soc. 2018;101(9):4108–4117.

10. Wu J, Xiao D, Wang Y, Wu L, Jiang Y, Zhu J. K/Na ratio dependence of the electrical properties of $[(K_xNa_{1-x})_{0.95}Li_{0.05}](Nb_{0.95}Ta_{0.05})O_3$ lead-free ceramics. J Am Ceram Soc. 2008;91(7):2385–7.
11. Feng S, Xiao D, Wu J, Li F, Xiao M, Zhu J. Influence of K/Na ratio on phase structure and electrical properties of $0.96(K_xNa_{1-x})NbO_3$-$0.04(Bi_{0.5}Na_{0.5})ZrO_3$ lead-free ceramics.J. Electroceramics. 2014;34(2–3):142–9.
12. Kang Y, Zhao Y, Huang R, Zhao Y, Zhou H. Effect of changing Na/K ratio on structure and electrical properties of $(Na_xK_y)(Nb_{0.885}Sb_{0.08})$-$0.035LiTaO_3$ lead-free piezoelectric ceramics. J Am Ceram Soc. 2011;94(6):1683–6.
13. Hao J, Bai W, Shen B, Zhai J. Improved piezoelectric properties of $(K_xNa_{1-x})_{0.94}Li_{0.06}NbO_3$ lead-free ceramics fabricated by combining two-step sintering.J. Alloy Compd. 2012;534:13–9.
14. Shannon RD. Revised effective ionic radii and systematic studies of interatomic distances in halides and chalcogenides. Acta Crystallogr A. 1976;32(5):751–67.
15. Fu J, Zuo R, Xu Z. High piezoelectric activity in (Na, K)NbO3 based lead-free piezoelectric ceramics: contribution of nanodomains. Appl Phys Lett. 2011;99(6):062901.
16. Damjanovic D. Contributions to the piezoelectric effect in ferroelectric single crystals and ceramics. J Am Ceram Soc. 2005;88(10):2663–76.
17. Kuwata J, Uchino K, Nomura S. Electrostrictive coefficients of Pb $(Mg_{1/3}Nb_{2/3})O_3$ ceramics. Jpn J Appl Phys. 1980;19(11):2099–103.
18. Huan Y, Wang X, Shen Z, Kim J, Zhou H, Li L. Nanodomains in KNN- based lead- free piezoelectric ceramics: origin of strong piezoelectric properties. J Am Ceram Soc. 2014;97(3):700–3.
19. Kawada S, Kimura M, Higuchi Y, Takagi H. (K, Na)NbO3-based multilayer piezoelectric ceramics with nickel inner electrodes. Appl Phys Express. 2009;2(11):111401.
20. Liu C, Liu P, Kobayashi K, Randall CA. Base metal co-fired (Na, K)NbO3 structures with enhanced piezoelectric performance. J Electroceramics. 2014;32(4):301–6.
21. Kobayashi K, Doshida Y, Mizuno Y, Randall C A. Possibility of cofiring a nickel inner electrode in a $(Na_{0.5}K_{0.5})NbO_3$-LiF piezoelectric actuator. Jpn J Appl Phys 2013;52(9S1):09KD07.
22. Liu H, Veber P, Rödel J, Rytz D, Fabritchnyi PB, Afanasov MI, et al. High-performance piezoelectric (K, Na, Li)(Nb, Ta, Sb)O3 single crystals by oxygen Annealing. Acta Mater. 2018;148:499–507.
23. Cen Z, Wang X, Huan Y, Zhen Y, Feng W, Li L. Defect engineering on phase structure and temperature stability of KNN-based ceramics sintered in different atmospheres. J Am Ceram Soc. 2018;101(7):3032–43.
24. Wang L, Ren W, Ma W, Liu M, Shi P, Wu X. Improved electrical properties for Mn-doped lead-free piezoelectric potassium sodium niobate ceramics. AIP Adv 2015;5(9):097120.
25. Rafiq MA, Tkach A, Costa ME, Vilarinho PM. Defects and charge transport in Mn-doped $K_{0.5}Na_{0.5}NbO_3$ ceramics. Phys Chem Chem Phys. 2015;17(37):24403–11.
26. Rafiq MA, Costa ME, Tkach A, Vilarinho PM. Impedance analysis and Conduction mechanisms of lead free potassium sodium niobate (KNN) single crystals and polycrystals: a comparison study. Cryst Growth Des. 2015;15(3):1289–94.
27. Sharma S, Kumari S, Rai R, Sharma DK. Effect of Na on the structural and electrical properties of lead-free sodium potassium niobate ceramics. Integr Ferroelectr. 2016;168(1):115–29.
28. Amaral L, Fernandes M, Reaney IM, Harmer MP, Senos AMR, Vilarinho PM. Grain growth anomaly and dielectric response in Ti-rich strontium titanate ceramics. J Phys Chem C. 2013;117(47):24787–95.
29. Tkach A, Amaral L, Vilarinho PM, Senos AMR. Oxygen vacancies as a link between the grain growth and grain boundary conductivity anomalies in titanium-rich strontium titanate. J Eur Ceram Soc. 2018;38(6):2547–52.
30. Yoon S-H, Randall CA, Hur K-H. Effect of acceptor (Mg) concentration on the resistance degradation behavior in acceptor (Mg)-Doped $BaTiO_3$ bulk ceramics: I. impedance analysis. J Am Ceram Soc. 2009;92(8):1758–65.

SUPPORTING INFORMATION

Additional supporting information may be found online in the Supporting Information section at the end of the article.

How to cite this article: Cen Z, Zhen Y, Feng W, et al. Phase transition, microstructure and electrical properties of $K_{1-x}Na_xNbO_3$-based ceramic sintered in reducing atmosphere. *J Am Ceram Soc*. 2019;102:3588–3597. https://doi.org/10.1111/jace.16231